J Solid State Electrochem (2000) 4: 168–176

ORIGINAL PAPER

Anabela Gomes · M. Helena Mendonça
M. Isabel da Silva Pereira · Fernanda M.A. Costa

Iron sulfide electrodeposits: effect of heat treatment on composition and structure

Received: 1 March 1999 / Accepted: 3 June 1999

Abstract Iron sulfide thin films were prepared by pulsed electrolysis on titanium substrates from aqueous solutions containing sulfur and iron sulfate, at 333 K. Annealing of the electrodeposits was performed under nitrogen, at different temperatures ranging from 523 to 773 K. By using solid state characterization techniques (X-ray diffraction and scanning electron microscopy/energy dispersive spectroscopy), the influence of the annealing temperature on the morphological and structural properties of the electrodeposits has been investigated. For all the studied temperatures, more than one phase was always obtained.

Key words Iron Sulphides · Pulsed Electrolysis · Annealing

Introduction

Iron and sulfur form a great variety of metallic and semiconducting compounds with a tendency towards some non-stoichiometry. Thus pyrite (FeS_2), pyrrhotite ($Fe_{1-x}S$), mackinawite (FeS_{1-x}) and troilite (FeS) are very important in various fields such as environment, energy production and also metallurgy. In recent years, many of these compounds have been investigated owing to their potential applications, particularly in photovoltaics and photoelectrocatalysis (pyrite) [1, 2], lithium batteries (pyrite and monosulfides) [3], electrocatalyst coatings for hydrogen evolution (monosulfides) [4, 5] and oxygen reduction (pyrite) [6]. Information on the composition, crystal structure, electrical properties and thermal stability of some mineral iron sulfides is presented in Table 1.

Iron sulfides are low cost materials of low toxicity and the future of their applications depends on the ability to produce them with controlled composition and properties, using inexpensive and reliable techniques. Electrochemical methods meet some of these requirements, since they are economical and versatile techniques for the preparation of thin films of high purity. Moreover, they are quickly scaled up to industrial production, offering inexpensive methods to produce large area samples. These are some of the reasons that make these methods so popular. However, electrodeposited films have some specific limitations such as non-stoichiometry, low crystallinity, high porosity and small grain size. In order to improve the quality of the films, electrodeposition is often associated with a subsequent thermal treatment performed either in the open air or in a controlled atmosphere.

The goal of the present paper is to report the investigation of the formation of iron sulfide films electrodeposited on titanium by pulsed electrolysis and discuss the role of the thermal treatment on the modifications of the film properties, namely crystal structure and composition.

A. Gomes · M.H. Mendonça · M.I. da Silva Pereira (✉)
F.M.A. Costa
Departamento de Química e Bioquímica,
Centro de Ciências Moleculares e Materiais,
Faculdade de Ciências,
Universidade de Lisboa, Campo Grande,
P-1749-016 Lisbon, Portugal
e-mail: misp@fc.ul.pt
Tel.: +351-1-7500109; Fax: +351-1-7500088

Experimental

The films were electrodeposited using a conventional three-electrode cell containing a commercial saturated calomel electrode (SCE) as a reference and a platinum mesh as counter electrode. The cell was connected to an EG&G PAR model 263 potentiostat and a Philips model PM 8271 XY-t recorder. The working electrode was a titanium disc (Goodfellows, 99.6% purity) of 10 mm diameter. Before the deposition, the titanium electrode was polished with abrasive paper and degreased with acetone followed by etching in a mixture of H_2SO_4 and HNO_3 and finally thoroughly washed with Millipore water.

The deposition bath was an aqueous 3:1 mixture of 0.35 mol dm^{-3} $Na_2S_2O_3$ and 0.01 mol dm^{-3} $(NH_4)_2Fe(SO_4)_2$ with the pH adjusted to 3 with H_2SO_4. All solutions were prepared from pro analysi grade chemicals dissolved in Millipore water and degassed with nitrogen.

Table 1 Some mineral iron sulfides and their properties [7–9]

Composition (mineral)	Crystal structure	Electrical properties	Thermal stability
FeS_2 (pyrite)	Cubic (pyrite type) a = 0.542 nm	Semiconductor	< 1015 K
Fe_3S_4 (greigite)	Spinel type, cubic a = 0.988 nm	Metallic conductor	Metastable (~453–473 K)
FeS_{1-x} (mackinawite)	Tetragonal a = 0.360 nm c = 0.503 nm	Semiconductor or metallic conductor	Metastable
$Fe_{1-x}S$,1C (pyrrhotite)	Hexagonal a = 0.698 nm c = 0.576 nm	Metallic conductor	1363 K
Fe_7S_8 (pyrrhotite)	Monoclinic a = 1.19 nm b = 0.686 nm c = 2.279 nm β = 90°26′	Metallic conductor	~527 K Metastable
FeS (troilite)	Hexagonal a = 0.597 nm c = 1.175 nm	Metallic conductor	< 411 K
FeS_2 (marcasite)	Orthorhombic a = 0.444 nm b = 0.541 nm c = 0.338 nm	Semiconductor	Metastable

The deposition was carried out by pulsed electrolysis consisting of an anodic pulse (E_a = 0.050 V vs. SCE) followed by a cathodic one (E_c = −0.950 V vs. SCE), both pulses with a duration of 1 s, at a temperature 333 K, under magnetic stirring, over 3 h.

The as-deposited films were subsequently treated under a nitrogen atmosphere at temperatures ranging from 523 to 773 K. The effect of the heat treatment duration was studied for each temperature used.

The structural characterization of the electrodeposits was done by X-ray powder diffraction (XRD) using a Philips PW 1730 diffractometer with Cu Kα radiation. Scanning electron microscopy/energy dispersive spectroscopy (SEM/EDS) were used for the characterization of the films' surface using a JEOL (JSM35C)/NORAN (VOYAGER) system.

Results and discussion

Voltammetric studies

Cyclic voltammetric experiments were carried out at the titanium electrodes in the unstirred deposition bath at 393 K in the potential range from 0.400 to −1.000 V vs. SCE, and a representative voltammogram is shown in Fig. 1 (cycle no. 5). In the anodic scan a well-defined peak (A_2) develops between −0.100 V and 0.000 V and a shoulder appears at E ≈ −0.600 V (A_1). Successive potential cyclic scans between the same potential limits give rise to an enhancement of peak A_2 while peak A_1 remains almost constant in size. Concerning the cathodic scan, a much complex profile is obtained. A shoulder is observed at E ≈ −0.600 V (C_1) followed by a well-defined peak C_2 near −0.700 V and a shoulder C_3 at more negative potentials.

To establish the relationship between the different oxidation and reduction peaks, changes in the negative potential limit were carried out. The voltammetric profiles recorded for two negative potential limits are presented in Fig. 2. It can be seen clearly that the size and number of peaks depend on the potential value at which the sweep is reversed. These voltammetric profiles are qualitatively similar to those that we have obtained earlier for Ebonex electrodes in a similar bath at room temperature [10]. Hence the peak assignment was done by comparison of the present results with the results for the Ebonex electrodes.

It is generally accepted that the decomposition of thiosulfate ion in acidic solutions can be described by the following reaction [11–13]:

$$S_2O_3^{2-}(aq) + H^+(aq) \rightleftharpoons S(\text{colloidal}) + HSO_3^-(aq) \quad (1)$$

and at pH ≈ 3 equilibrium between HSO_3^- and H_2SO_3(aq) also occurs [14]. All these species exist in solution and from the estimated standard potential stability range, adjusted to the bath pH, it is expected that H_2SO_3 is the first to be reduced, followed by HSO_3^-, $S_2O_3^{2-}$ and colloidal sulfur [15, 16].

According to this, the cathodic wave observed at ≈ −0.300 V (C_0) was assigned to the reduction of the

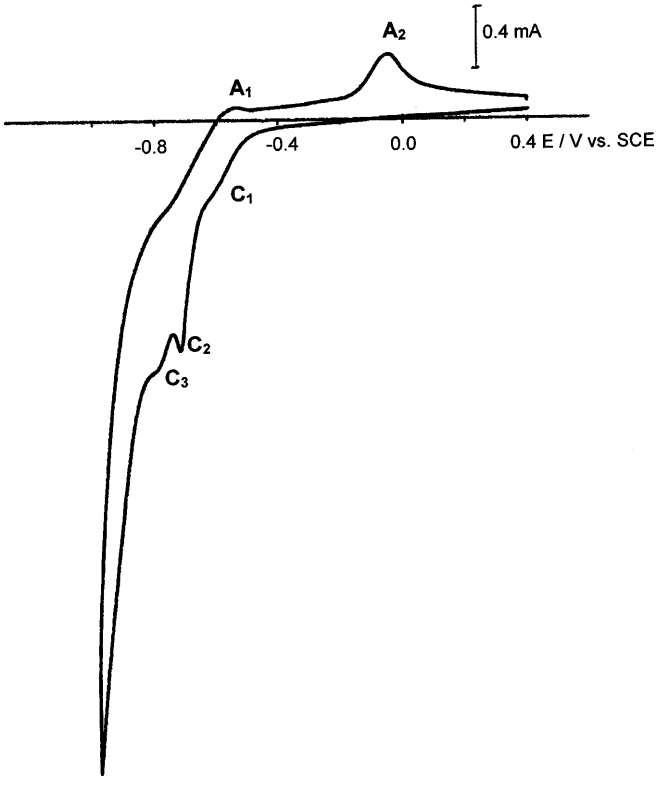

Fig. 1 Cyclic voltamogram (5th cycle) obtained for a Ti electrode in the unstirred deposition bath at 333 K in the potential range 0.400 V to −1.000 V vs. SCE. Sweep rate 10 mV/s. Electrode area 0.8 cm^2

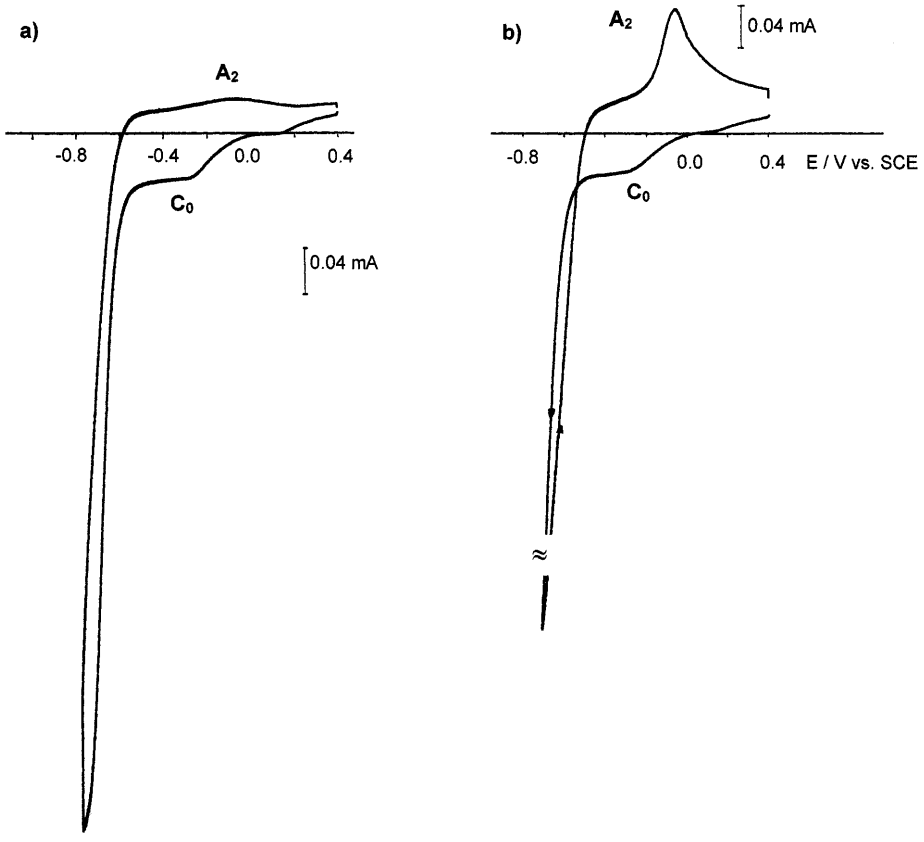

Fig. 2 Cyclic voltamograms obtained for a Ti electrode in the unstirred deposition bath at 333 K at different negative potential limits: **a** −0.800 V and **b** −0.900 V vs. SCE. Sweep rate 10 mV/s. Electrode area 0.8 cm^2

sulfur/oxygen-containing species (Fig. 2a) and the subsequent increase in current to the sulfur reduction, according to the following scheme [16]:

$$S + 2H^+ + 2e^- \rightarrow H_2S \quad (2)$$

In the same voltammogram, peak A_2 appears as a hump that develops into a well-defined peak when the potential limit is extended to more negative values (Figs. 1 and 2b). As before, this peak was assigned to the anodic formation of a sulfur layer [10, 17].

When the negative limit is set to −0.900 V (Fig. 2b), a current loop is observed on the cathodic scan. Current loops are currently associated either with nucleation processes or changes in the electrical properties of the films [18, 19]. In this system, both phenomena can take place: the nucleation of iron or iron sulfide films are thermodynamically possible in this potential range [20, 21] and a modification of the electrical resistivity of the film, due to the dissolution of the sulfur layer formed on the electrode, cannot be discarded. However, it seems more likely that a nucleation process happens, since a complete stripping of the sulfur layer has not been observed as the charges associated with the formation and dissolution peaks show.

According to the work of Aricó et al. [17] on the electrodeposition chemistry of the Fe-S system, the presence of sulfur on the electrode surface shifts negatively by about 0.150 V the reduction of Fe^{2+} to metallic iron. This result led us to associate the loop with the nucleation of iron sulfide film according to [22]:

$$Fe^{2+} + (1-x)H_2S \rightarrow FeS_{1-x} + 2H^+ \quad (3)$$

A voltammetric study of the system Fe(II)/Fe(Hg) in aqueous thiosulfate solutions of unspecified pH has been previously reported by Itabashi [23]. The formation of iron sulfide was claimed and a mechanism has been proposed for the film formation, involving the reduction of Fe(II) through the formation of a complex between Fe(II) and $S_2O_3^{2-}$ at the electrode surface. In the present study, no attempts have been made to extend the mechanism proposed by Itabashi for the film formation, since we are dealing with a solid titanium substrate and low pH.

As the negative potential limit increases to −1.000 V the anodic shoulder A_1 appears at ≈ −0.600 V and the cathodic profile shows the features already referred to in Fig. 1. The shoulder A_1, has been identified with the oxidation of metallic iron, formed during the cathodic sweep. The development of the sharp peak C_2 was assigned to the reduction of the sulfur deposited on the iron sulfide film, which is formed and not redissolved during the previous sweeps and it is logically described by the reaction of Eq. 2. The appearance of this peak after several scans (5–7) supports this assignment.

In Fig. 3, where the negative limit was set to −1.200 V, the effect of cycling is presented. During the initial scan in the negative going direction a broad cathodic peak was observed around −0.800 V and has been assigned to the reduction of a thin layer of adsorbed sulfur at the titanium electrode surface [24].

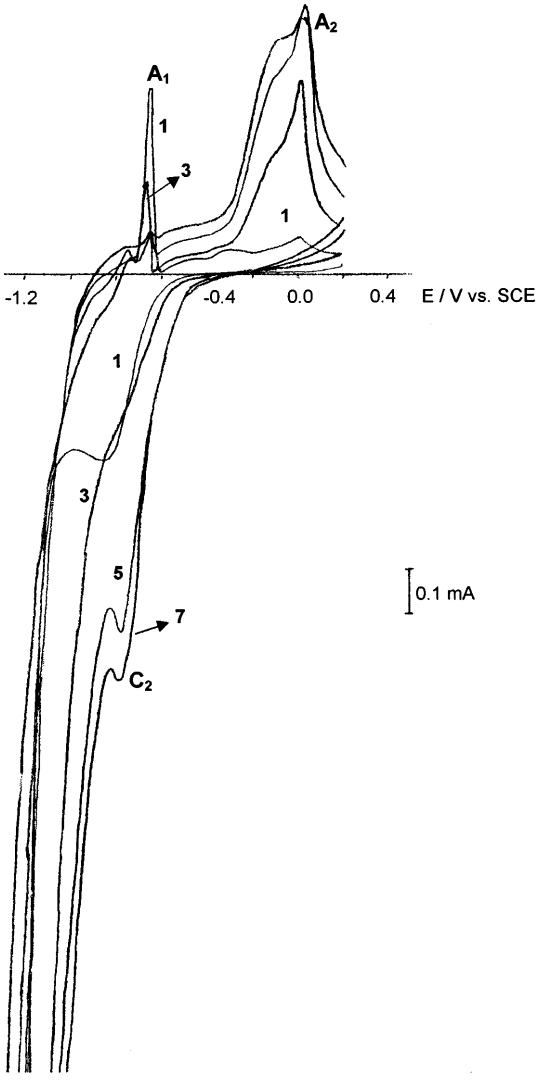

Fig. 3 Repetitive cyclic voltamograms obtained for a Ti electrode in the unstirred deposition bath at 333 K in the potential range 0.200 V to −1.200 V vs. SCE (the numbers in the figure correspond to the scan number). Sweep rate 10 mV/s. Electrode area 0.8 cm^2

During cycling this peak vanishes, giving rise to high negative currents and later on to peak C_2.

The deconvolution of peak A_1 into two peaks was observed for the initial runs and was interpreted as a consequence of different rates of reoxidation of metallic iron at the titanium electrode and at the electrode covered with iron sulfide. Similar results were obtained by us for the Ebonex electrodes [10], by Winkler et al. [25] for the Fe(II)-SCN^- system on a glassy carbon electrode and by Tacconi et al. [26] for iron sulfide on gold.

The increasing complexity of the anodic peak A_2 with cycling supports the hypothesis that, in addition to the back reaction (Eq. 2), peak A_2 should account for the iron sulfide film anodic dissolution according to

$$FeS_{1-x} \rightarrow Fe^{2+} + (1-x)S + 2e^- \quad (4)$$

or

$$FeS_{1-x} \rightarrow Fe^{3+} + (1-x)S + 3e^- \quad (5)$$

Similar schemes have been proposed by Hamilton and Woods [27] for the oxidation of pyrrhotite at pH 4.6 and by Ahlberg and Broo [6] for the anodic dissolution of pyrite at low pH. Studies on the oxidation of pyrrhotite surfaces in acidic medium show the formation of a sulfur enriched layer [28, 29].

The fact that peak A_1 does not increase with the number of cycles distinguishes it from peak A_2, and implies a passivating process due to film formation in addition to the decrease of Fe^{2+} species due to its consumption in the cathodic film formation. The high currents observed between peaks A_1 and A_2 suggest that anodic formation of the iron sulfide film occurs.

Electrodeposition and structural characterization of iron sulfide films

Electrodeposition conditions

The electrodeposition of iron sulfides was performed under potentiostatic conditions. The positive and negative potential values were chosen in accordance with the voltammetric data.

Electrolyses were performed with different positive (E_a = =0.000 and 0.050 V) and negative (E_c ranging from −0.900 to −1.150 V) potentials. The amount of the black deposit formed on the electrode surface was strongly influenced by the negative potential of the cycle, while the positive value had no significant effect on it.

XRD results of the deposit led us to optimize the electrodeposition conditions. Therefore, all subsequent experiments were carried out at the selected potential values of 0.05 V and −0.95 V vs. SCE for the positive and negative pulses, respectively.

Structural characterization of the as-deposited films

A XRD pattern of the as-deposited film is shown in Fig. 4a. Excluding the lines of the titanium substrate and support, the remaining diffraction lines are indexed as the mackinawite phase (FeS_{1-x}) according to the JCPDS file 24–73. The *d* spacing and *h*,*k*,*l* values for FeS_{1-x} are presented in Table 2. A good agreement between the experimental and calculated *d* values is observed for the crystalline phase.

In the literature, mackinawite is referred to as one of the iron monosulfides that has been synthesized at low temperature in aqueous solution [30]. References to its preparation at low temperatures over a wide range of pH values, in alkaline solutions [31] and at pH 3.3 [32], can be found in the literature.

On the other hand, studies on the electrochemical formation of mackinawite by anodic oxidation of iron in alkaline sulfide solutions have been reported by Shoesmith et al. [33] in the pH range 9–12 and Bezdicka et al.

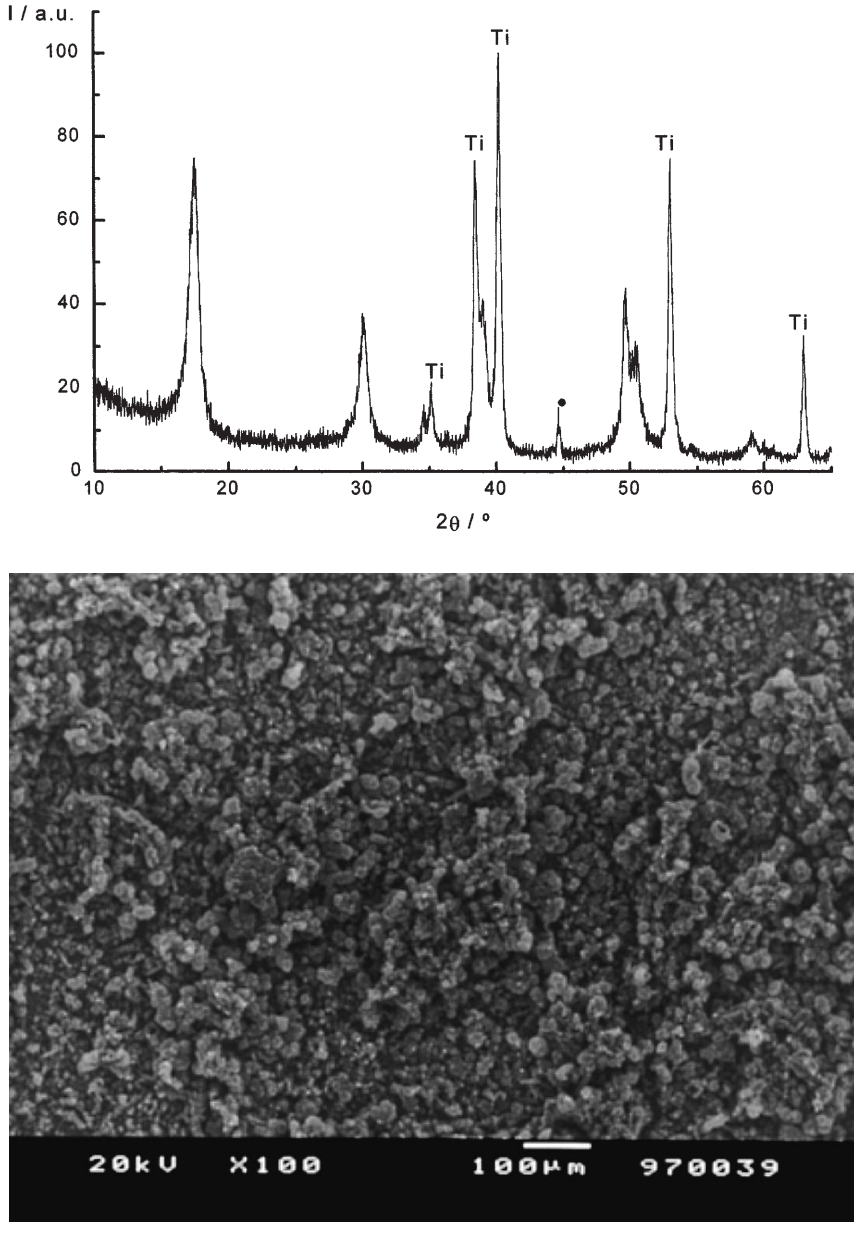

Fig. 4 **a** X-ray diffraction (XRD) pattern of the as-deposited film. The indicated diffraction lines are due to the substrate (Ti) and the sample holder (●). **b** Scanning electron micrograph of the as-deposited film

[34] found that the best pH for growing mackinawite was 7.8. However, studies on the corrosion of iron in aqueous H_2S solutions showed that mackinawite is formed as a corrosion product between pH 3 and pH 7 [35].

Table 2 *d* spacing and *hkl* for FeS_{1-x} ($x = 0.1$) mackinawite

h k l	d_{obs} (nm)	D_{calc} (nm)
001	0.50279	0.50332
101	0.29694	0.29667
110	0.25928	0.25968
111	0.23059	0.23078
200	0.18359	0.18362
112	0.18039	0.18072
211	0.15626	0.15614
220	0.12967	0.12984

It is interesting to note that mackinawite does not appear on the electrochemical equilibrium Eh-pH diagrams for the sulfur-iron-water system [22, 27, 36, 37]. Usually a domain of stability of FeS is shown without specification of the phase. Moreover, the stability regions also differ. As an example, the simplified Pourbaix diagram presented by Hemmingsen and Lima [36] shows that FeS is not stable below pH 4–4.5, while Biernat and Robins [22] derived another one where the domain of stability of FeS is extended to pH≈1. Under these conditions a thermodynamic analysis is very difficult. A possible explanation for the absence of mackinawite on the Eh-pH diagrams is its metastability [30].

In the present work the XRD results led us to conclude that the main component of the deposit is iron sulfide, with a tetragonal structure (according with the

JCPDS file 24–73, which corresponds to mackinawite with composition $FeS_{0.9}$).

The grain size of the mackinawite has been determined by the width and half height of the (001) diffraction line by applying the Scherrer equation and Warren method [38]. A median value of 9 nm was obtained. Values of the same order have been reported for very finely divided mackinawite prepared by anodic electrodeposition [39].

SEM shows (Fig. 4b) that the films are porous and present the same morphology all over the surface. However, EDS results give the information that some compositional heterogeneity occurs.

Film formation

According to the voltammetric data, during the negative pulse the sulfur and iron ions are reduced. Taking into account the value of the pulse potential, both iron metal and ions can coexist at the electrode surface. The iron sulfide film is formed during the course of the reduction of Fe(II), when sulfur undergoes electrochemical reduction. The electrochemical reaction of iron sulfide formation may be written as:

$$Fe^{2+} + (1-x)S + 2e^- \Rightarrow FeS_{1-x} \quad (6)$$

On the other hand, at the positive semicycles the oxidation of metallic iron takes place accompanied by the formation of a sulfur surface film, both processes being possibly mass-transfer limited owing to the value of the applied potential. This suits the small influence of the potential value of the positive pulse on the amount of electrodeposited film. Probably a small dissolution of the iron sulfide film can take place on the subsequent anodic pulse, according to reactions 4 and/or 5.

The lack of sulfur identification by XRD on the as-deposited films is probably due to its amorphous nature.

The thickening of the film results from the formation of successive layers of iron sulfide. The deposition of intermediary metal and/or sulfur-enriched layers should be considered. Evidence of sulfur-rich layers comes from the SEM/EDS results. Values for the atomic ratio S/Fe ranging from 1.05 to 1.51 were obtained. Also the voltammetric charges involved in the sulfur formation/dissolution process point to the presence of enriched sulfur layers.

Thermal treatment of the deposited films

The as-deposited films were annealed for 1 h at different temperatures, from 523 to 773 K in a nitrogen atmosphere, in order to minimize the sample oxidation. The films were identified by powder XRD, for each annealing temperature. Figure 5 shows the XRD spectra obtained for the samples annealed at 523, 673 and 773 K, which represent the final products.

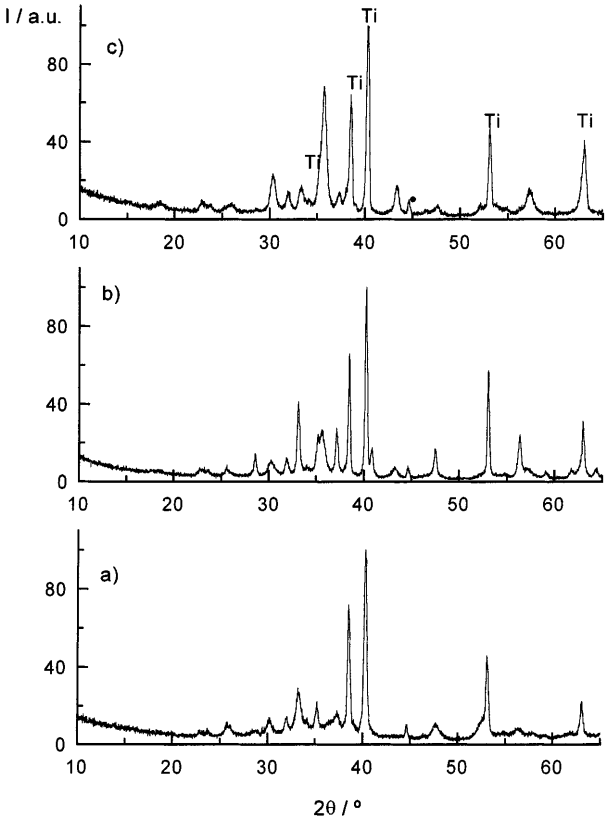

Fig. 5 XRD patterns of the as-deposited films after annealing in a nitrogen atmosphere at **a** $T = =523$, **b** $T = =673$ and **c** $T = =773$ K for 1 h. The indicated diffraction lines are due to the substrate (Ti) and the sample holder (●)

Examination of these patterns shows that the number, intensity and position of the diffraction lines are affected by the heat treatment, which led us to conclude that the annealing temperature plays an important role in the film characteristics. Moreover, the formation of new phases occurs and the film crystallinity improves.

The analysis of the XRD patterns revealed that the film is a mixture of phases with a composition depending on the final heating temperature. For the three mentioned temperatures the *d* spacing values for each phase were determined and compared with the values given in JCPDS [40] according to Table 3. The general features of the results are summarized in Table 4, where the presence of greigite (G), pyrite (Py), pyrrhotite (Po) and iron oxide for the various samples is shown.

A qualitative discussion based on the observed modifications induced in the films by the thermal treatment is now attempted. As previously stated, the as-deposited film consists of mackinawite and amorphous sulfur; however, when the annealing temperature increases, new phases richer in sulfur than mackinawite are formed. At increased annealing temperatures the sulfur could diffuse into the films and react, giving rise to new phases richer in sulfur. Table 4 shows that pyrite and pyrrhotite are present at all annealing temperatures, pyrite being the dominant phase from 523 to 673 K. Greigite is only

Table 3 *d*-spacing and phases identified for the different annealing temperatures

T = 523 K				T = 673 K				T = 773 K			
d_{obs} (nm)	Identified phases			d_{obs} (nm)	Identified phases			d_{obs} (nm)	Identified phases		
0.346	G			0.376		Fe_2O_3		0.478	Fe_2O_3		
0.311		Py		0.348		Fe_2O_3		0.374	Fe_2O_3		
0.296	G		Po	0.312	Py			0.342	Fe_2O_3		
0.269		Py		0.295		Fe_2O_3	Po	0.295	Fe_2O_3		Po
0.262			Po	0.280		Fe_2O_3		0.279	Fe_2O_3		
0.246	G			0.270	Py			0.269		Py	
0.241		Py		0.263			Po	0.263			Po
0.191	G	Py		0.252		Fe_2O_3		0.251	Fe_2O_3		
0.163		Py		0.242	Py			0.241		Py	
0.159			Po	0.220	Py			0.208	Fe_2O_3		Po
0.156		Py		0.209		Fe_2O_3	Po	0.190		Py	
0.150	G	Py		0.191	Py			0.175	Fe_2O_3		Po
				0.167		Fe_2O_3		0.167	Fe_2O_3		
				0.163	Py			0.163		Py	
				0.161		Fe_2O_3	Po	0.161	Fe_2O_3		Po
				0.156	Py						
				0.150	Py						
				0.144	Py		Po				

Table 4 Phases identified for the different annealing temperatures (dominant phase represented bold)

T (K)	Identified phases
523	FeS_2, $Fe_{1-x}S$, Fe_3S_4
623	FeS_2, $Fe_{1-x}S$, Fe_3S_4
673	FeS_2, $Fe_{1-x}S$, Fe_2O_3
723	FeS_2, $Fe_{1-x}S$, Fe_2O_3
773	FeS_2, $Fe_{1-x}S$, Fe_2O_3

present for $T \leq 623$ K and iron oxide for $T \geq 673$ K, being the dominant phase for 723 K and 773 K.

Considering the conversion of mackinawite, it can occur in different ways, depending on the experimental conditions. Takeno et al. [31] and Lennie et al. [41] found that when pure mackinawite is heated in an evacuated system up to 443 K, just hexagonal pyrrhotite is obtained. However, in the presence of elemental sulfur or oxygen, mackinawite converts to greigite according to the respective I and II mechanisms proposed by Rickard [42] and Taylor et al. [39]:

$$\text{I}\quad 3FeS_{1-x} + (1+3x)S \rightarrow Fe_3S_4 \tag{7}$$

$$\text{II}\quad 3FeS_{1-x} + 2O_2 \rightarrow Fe_3O_4 + [(3-3x)/8]S_8 \tag{8}$$

$$2FeS_{1-x} + [(1+3x)/8]S_8 \rightarrow Fe_3S_4 \tag{9}$$

In the experiments carried out, the conversion of mackinawite to pyrrhotite and greigite is in accordance with the literature.

Pyrite is identified as a product at all annealing temperatures. The XRD patterns show that the films annealed at $T \leq 673$ K are rich in the pyrite phase, while those annealed at higher temperature have an oxide phase dominant.

Willkin and Barnes [43] assumed that greigite is an intermediate in the formation of pyrite with framboidal morphology, i.e. a pyrite with a raspberry-like morphology. An aggregation model via greigite as a precursor can explain the formation of the so-called framboidal pyrite. This conversion can be envisaged as an addition of solid elemental sulfur according to the redox reaction:

$$Fe_3S_4(s) + 2\,S(s) \rightarrow 3\,FeS_2(s) \tag{10}$$

At 673 K, all greigite has been converted to pyrite and the presence of Fe_2O_3 is detected. The oxide formation should be linked to OH groups retained inside the film, combined with oxidation due to air exposure of the polycrystalline film. FeO(OH) converts to Fe_2O_3 by heating [44].

Figure 6 shows the grain size variation of the pyrite phase on the films with the annealing temperature for 1 h. It can be seen that the annealing temperature plays a substantial role in the grain size. It is interesting to note that a maximum value is reached at T = 673 K,

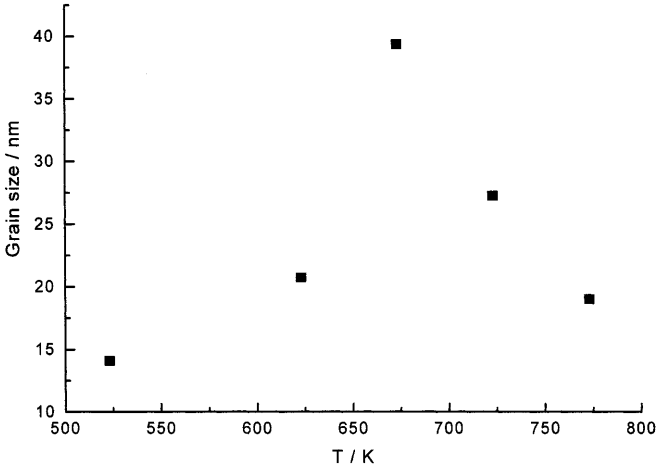

Fig. 6 Grain size dependence on the annealing temperature for the FeS_2 phase

precisely the temperature limit at which the pyrite powder is stable [45]. The grain size decrease at $T > 673$ K can be understood as an inhibition of the growth process of the pyrite grains by the oxide.

SEM/EDS studies of samples annealed at 673 K during 1 h reveal S/Fe atomic ratio values around 0.9, decreasing to 0.2 when the annealing is performed for 4 h. These results point to pyrite decomposition at $T > 673$ K according to

$$FeS_2(s) \rightarrow FeS(s) + 1/2S_2(g) \quad (11)$$

This assumption is in accordance with the gradual weakening of the pyrite XRD lines observed with the increasing heating time, while those of iron oxide show higher intensities (Fig. 7). Figure 8 shows the evolution of the intensity maximum line for the pyrite and iron oxide phases, with the annealing time. These results underline the importance of the annealing time on the preparation of the films. At prolonged time, sulfur can escape and simultaneously the crystallinity of the existing oxide improves.

Conclusion

Mackinawite was prepared by electrochemical deposition in acidic aqueous solutions. Tailoring of the composition was achieved by the annealing treatment, in spite of its close dependence of the deposition conditions, mainly the sulfur deposited on the anodic semicycle. The results presented clearly show the importance of the annealing treatments for the film structure and stoichiometry and they are summarized by Scheme 1.

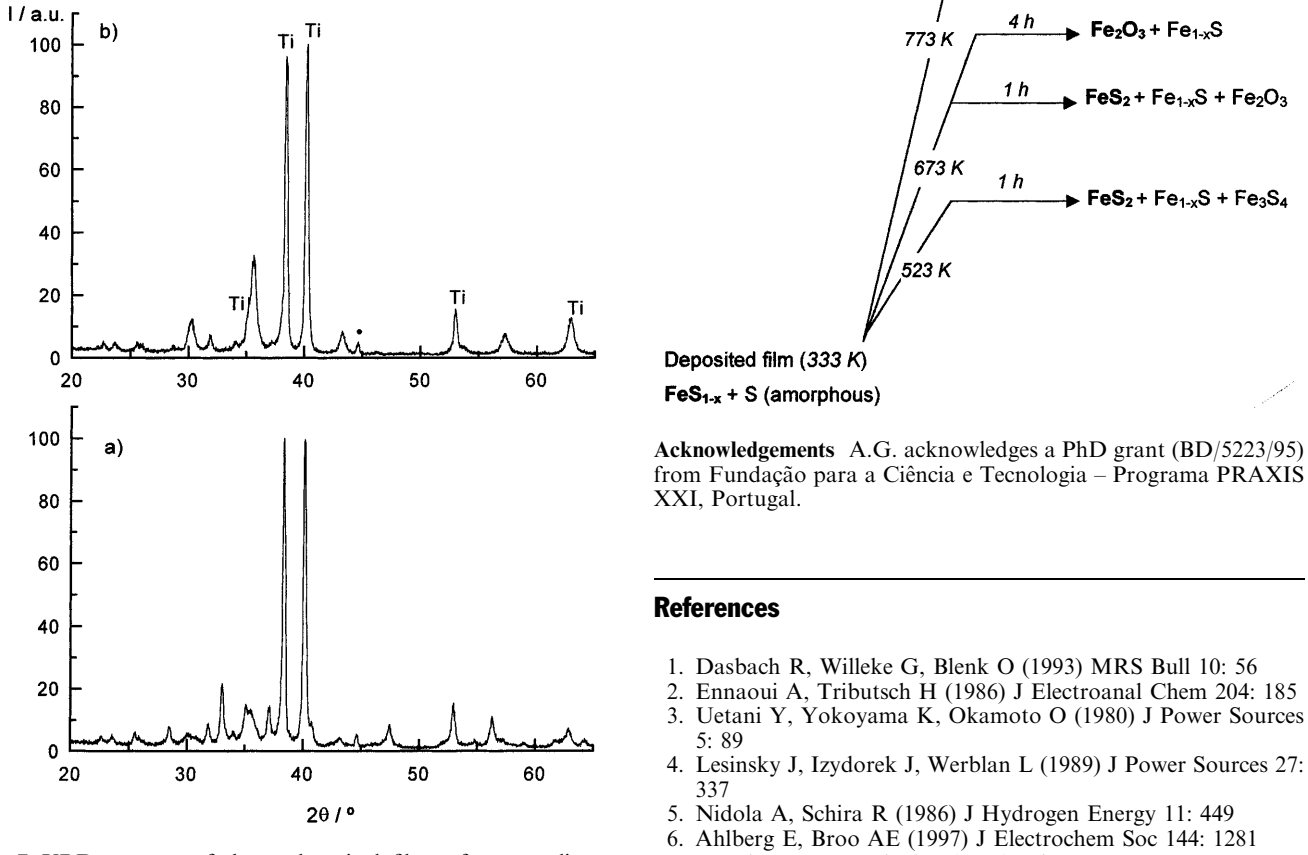

Fig. 7 XRD patterns of the as-deposited films after annealing at 673 K for **a** 1 h and **b** 4 h. The indicated diffraction lines are due to the substrate (Ti) and the sample holder (●)

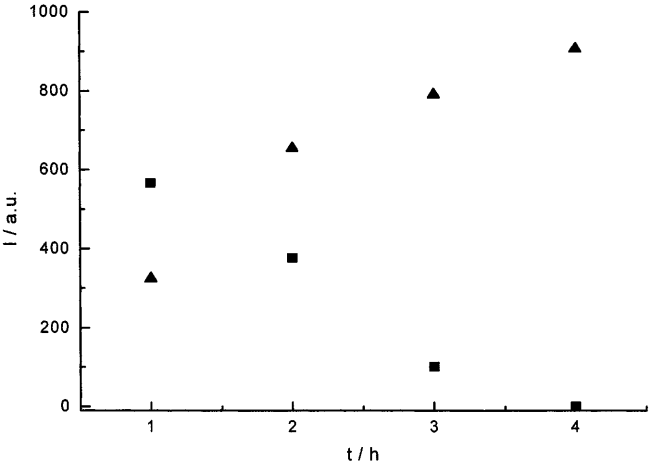

Fig. 8 Evolution of the intensity maximum reflexion with heating time for the FeS_2 (■) and Fe_2O_3 (▲) phases

Acknowledgements A.G. acknowledges a PhD grant (BD/5223/95) from Fundação para a Ciência e Tecnologia – Programa PRAXIS XXI, Portugal.

References

1. Dasbach R, Willeke G, Blenk O (1993) MRS Bull 10: 56
2. Ennaoui A, Tributsch H (1986) J Electroanal Chem 204: 185
3. Uetani Y, Yokoyama K, Okamoto O (1980) J Power Sources 5: 89
4. Lesinsky J, Izydorek J, Werblan L (1989) J Power Sources 27: 337
5. Nidola A, Schira R (1986) J Hydrogen Energy 11: 449
6. Ahlberg E, Broo AE (1997) J Electrochem Soc 144: 1281
7. Vaughan DJ, Lennie AR (1991) Sci Prog 75: 371
8. Ribbe PH (ed) (1976) Sulfide mineralogy reviews in mineralogy, vol 1. Mineralogy Society of America, Washington

9. Vaughan DJ, Craig JR (1978) Mineral chemistry of metal sulfides. Cambridge University Press, Cambridge
10. Gomes A, Silva Pereira MI, Mendonça MH, Costa FMA (1995) J Appl Electrochem 25: 1045
11. Johnston F, McAmish L (1973) J Colloid Interface Sci 42: 112
12. Power GP, Peggs DR, Parker AJ (1981) Electrochim Acta 26: 681
13. Fatas E, Herrasti P, Arjona F, Camarero EG (1987) J Electrochem Soc 134: 2799
14. Hemmingsen T (1992) Electrochim Acta 37: 2785
15. Hemmingsen T (1992) Electrochim Acta 37: 2775
16. Biernat RJ, Robins RG (1969) Electrochim Acta 14: 809
17. Aricó AS, Antonucci V, Antonucci PL, Cocke DL, Giordano N (1991) Electrochim Acta 36: 581
18. Pereira MIS, Silva MFG, Costa FMA (1984) J Electroanal Chem 172: 367
19. Silva Pereira MI, Peter LM (1982) J Electroanal Chem 131: 167
20. Pourbaix M (1974) Atlas of electrochemical equilibria in aqueous solutions. NACE, Houston, TX
21. Licht S (1988) J Electrochem Soc 135: 2971
22. Biernat RJ, Robins RG (1969) Electrochim Acta 17: 1261
23. Itabashi E (1979) J Electroanal Chem 103: 189
24. Hamilton IC, Woods R (1983) J Appl Electrochem 13: 783
25. Winkler K, Kalinowski S, Krogulec T (1988) J Electroanal Chem 252: 303
26. Tacconi NR, Medvedko O, Rajeshwar K (1994) J Electroanal Chem 379: 545
27. Hamilton IC, Woods R (1981) J Electroanal Chem 118: 327
28. Jones CF, LeCount S, Smart RStC, White TJ (1982) Appl Surf Sci 55: 65
29. Mycroft JR, Bancroft GM, McIntyre NS, Lorimer JW, Hill IR (1990) J Electroanal Chem 292: 139
30. Taylor P (1980) Amer Mineral 65: 1026
31. Takeno S, Zôka H, Niihara T (1970) Am Mineral 55: 1639
32. Berner RA (1967) Am J Sci 265: 773
33. Shoesmith DW, Bailey MG, Ikeda B (1978) Electrochim Acta 23: 1329
34. Bezdicka P, Grenier JC, Fournés L, Wattiaux A, Hagenmuller P (1989) Eur J Solid State Inorg Chem 26: 353
35. Shoesmith DW, Taylor P, Bailey MG, Owen DG (1980) J Electrochem Soc 127: 1007
36. Hemmingsen T, Lima H (1998) Electrochim Acta 43: 35
37. Garrels RM, Christ CL (1965) Solutions, minerals and equilibria. Harper and Row, NY
38. Cullity BD (1978) Elements of X-ray diffraction. Addison-Wesley, New York
39. Taylor P, Rummery TE, Owen DG (1979) J Inorg Nucl Chem 41: 596
40. JCPDS, International Center for Diffration Data (1988) Powder diffraction files: 16–713, 42–1340, 25–411, 25–1402. Swarthmore, USA
41. Lennie AR, England KER, Vaughan D (1995) Am Mineral 80: 960
42. Rickard D, Schoonen MAA, Luther III GW (1995) Chemistry of iron sulfides in sedimentary environmental . . . . In: Vairavamurthy V, Schoonen MAA (eds) A Chemical Society Symposium Series, vol 612. chap IX, p 168
43. Wilkin RT, Barnes HL (1997) Geochim Cosmochim Acta 61: 323
44. Cotton FA, Wilkinson G (1996) Advanced inorganic chemistry. Interscience, New York
45. Ennaoui A, Tributsch H (1993) Sol Energy Mater 29: 289